JOURNAL OF AIRCRAFT
Vol. 50, No. 2, March–April 2013

Nonlinear Analysis of Aeroservoelastic Models with Free Play Using Describing Functions

Brian Danowsky* and Peter M. Thompson†
Systems Technology, Inc., Hawthorne, California 90250
and
Sunil Kukreja‡
NASA Dryden Flight Research Center, Edwards, California 93560

DOI: 10.2514/1.C031370

Nonlinearities in aeroservoelastic systems are a source of limit-cycle oscillations. Aerodynamic control surfaces and actuators may have excessive free play in connecting joints and hinges, which has the potential to cause limit-cycle oscillations associated with aeroservoelastic vibrations, impacting handling and ride quality and leading to structural fatigue. Because of these negative impacts, free-play limits have been established by the Joint Services Guidance Military Specification. These military specifications have also been adopted by the Federal Aviation Administration for commercial aircraft. This stringent requirement can be excessively conservative and is very difficult and costly to meet. Analytical tools using describing functions have been developed to establish free-play limits on aeroservoelastic aircraft systems without adverse consequences. These tools are robust and easy to implement, justifying relaxation or validation of the conservative requirements. It is shown that oscillation frequency and amplitude can be accurately estimated using describing functions with an analytical model of an aeroservoelastic system with free play. A novel analysis technique is also demonstrated, whereby free-play occurrence and limit-cycle behavior can be visualized using time-varying frequency content. Validation of the method is illustrated with an aeroservoelastic stabilator control surface model using nonlinear simulation, with free-play limits found in experimental conditions.

I. Introduction

Aerodynamic control surfaces with excessive free play may cause limit-cycle oscillations (LCO), a sustained vibration of constant amplitude. An LCO is caused by a combination of aeroservoelastic effects and free play. If the amplitude is sufficiently large, it can impact handling and ride quality, leading to structural fatigue and ultimately structural failure. LCO phenomenon due to free play has been shown to exist through flight tests, wind-tunnel tests [1,2], and analytical studies.

Free-play limits have been established by the Joint Service Guidance Military Specification [3] for all movable control surfaces to alleviate LCO and assure that failure due to this phenomenon is avoided. The Federal Aviation Administration (FAA) has adopted the same military requirements for commercial aircraft. Free play is typically distributed throughout the actuator and control surface. Contributions from the actuator mounting bearings and surface hinge are shown as examples in Fig. 1a [4]. The requirement is stringent and in many cases it is overly conservative. The requirement can be extremely difficult (in some cases impossible) to meet and, as such, increases the cost of manufacturing. Existing free-play limits (e.g., control surface deflection angle) must be constantly monitored throughout the life of the aircraft to ensure the specification is not violated. Currently, the monitoring method is labor intensive and involves statically loading the surface and measuring the control surface deflection while on the ground. This adds costs associated with inspection. A typical measurement setup and result are shown in Figs. 1b and 1c, respectively [5].

Because of conservative control surface free-play specifications, a legitimate and reliable analytical technique to analyze the effect of control surface free play is desirable. Reliable analytical techniques can be used in early design phases, relaxing the free-play requirement and ultimately reducing aircraft weight, as well as manufacturing and inspection costs.

Describing functions are a classical approach to analyzing nonlinearities in dynamic systems [6]. A describing function implements quasi-linear elements to represent nonlinearities, facilitating complex analysis (i.e., stability prediction, performance, limit-cycle occurrence, and amplitude). It is shown that free play, with magnitude comparable to that found in experimental or commercial applications, can be accurately represented via describing function analysis. A generic aeroservoelastic stabilator model with free play was constructed using linear finite elements (FEs) and unsteady doublet-lattice-based aerodynamics. Nonlinearities in the form of free play are separated from the model using linear fractional transformations (LFT), casting the problem into a structure of significant generality. Using this model form, the effects of free play on stability, performance, and limit cycles can be analyzed using describing functions with high accuracy. Nonlinear simulations of the aeroservoelastic stabilator model verify the efficacy of the developed technique.

II. Free-Play Nonlinearity and Describing Function Description

The free-play nonlinearity (Fig. 2a) is a piecewise linear function. This nonlinearity is also commonly referred to as threshold and dead zone, among others. Free play is a static (memoryless) nonlinearity. The output of a static nonlinearity at time t depends only on the input value at the same time. This property provides that the so-called describing function approximation is a gain with no phase shift and is frequency independent [6]. This is often referred to as a "simple nonlinearity."

Using an accurate describing function, considerable insight can be gained from quasi-linear analysis. The free-play nonlinearity is replaced by a gain reduction, and predictions about nonlinear behavior, including LCO, are made using the resulting quasi-linear model. Gain reduction is heavily dependent on the input and, therefore, the quasi-linear approach of describing function analysis assumes generalized inputs.

Presented as Paper 2010-492 at the 48th AIAA Aerospace Sciences Meeting, Orlando, FL, 4–7 January 2010; received 12 January 2011; revision received 23 February 2012; accepted for publication 24 February 2012; published online 24 January 2013.

*Principal Research Engineer. Senior Member AIAA.
†Ph.D., Chief Scientist. Senior Member AIAA.
‡Ph.D., Aerospace Research Engineer. Member AIAA.

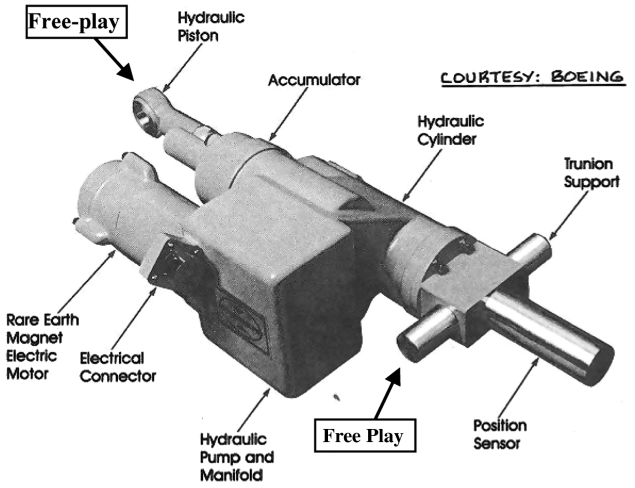

a) Typical electrohydrostatic actuator and probable free-play locations

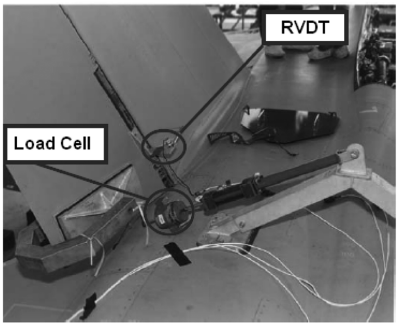

b) Measurement setup

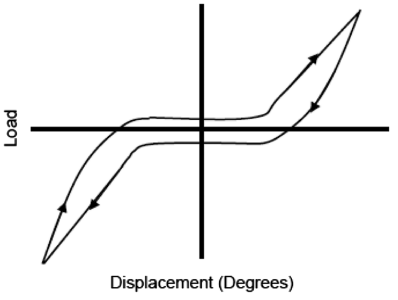

c) Typical free-play measurement

Fig. 1 Typical free-play measurement setup (courtesy of Boeing [5]).

As stated, the describing function for free play is sufficiently represented as a gain reduction because it is a static function. The amount of gain reduction depends on the ratio a/A, where a is free-play size and A is signal amplitude. For signals that are sinusoidal, the parameter A is the peak magnitude, and for stochastic signals, A is the standard deviation. As such, the describing function gain reduction for free play can be quantified accurately (Fig. 2c). Notice the curve is higher for the Gaussian case because the output is zero for a sine wave with amplitude less than a, but nonzero for a random signal with a standard deviation less than a. In either case, when $a/A \ll 1$, the gain reduction is very small and free play has little effect. When $a/A \cong 1$ (sinusoidal) and $a/A \cong 2$ (Gaussian), the gain is zero or close to it because free play dominates the response.

A limit-cycle prediction is made if gain reduction results in instability. Define the describing function $\alpha = f(a/A)$ and its inverse function as $a/A = finv(\alpha)$. If gain reduction α results in an unstable system, then a limit cycle is predicted with magnitude $A = a/finv(\alpha)$. This is qualitatively described as follows:

1) Small gain reduction $\alpha \approx 1$: If gain reduction causes instability that is not large, then $finv(\alpha) \ll 1$ and $A \gg a$. The resulting limit-cycle amplitude is much larger than the size of the free play.

2) Large gain reduction $\alpha \ll 1$: If a large gain reduction is required for instability, which is often the case, then $finv(\alpha) \approx 1$ and $A \approx a$. The limit-cycle amplitude is about the same size as the free play.

In both cases, a gain reduction is required and, therefore, the system containing free play must be conditionally stable with respect to its describing function gain, providing observability for a limit cycle to be predicted. The negative inverse describing function represented on a Nichols chart is a traditional tool for limit-cycle prediction. For simple nonlinearities, such as free play, gain reduction requirements may be predicted using simpler tools, such as root locus $j\omega$ crossovers and Bode -180 deg crossovers.

III. Generic Stabilator Model

A generic stabilator model was constructed using finite elements and unsteady doublet-lattice aerodynamics. The stabilator constructed represents a 4.5 ft half-span wing with a taper ratio of 0.55 and a leading-edge sweep angle of -45 deg (backward sweep). This wing was connected to a single hinge at a location on the root chord. A spring or a more complicated system (e.g., an actuator) can be connected between the hinge and ground. Free play may be supplied at various points throughout the connection for analysis.

A. Structural Finite Element Model

The main structure is composed of quadrilateral plate elements (local mass and stiffness matrices based on Przemieniecki [7]). These local elements have four coplanar nodes that are restricted to out-of-plane translation and in-plane rotation, limiting the degrees of freedom to 12 per element. This element is well suited for coplanar wings that exhibit bending and twisting motion characteristics of how the stabilator is expected to behave. The wing plate elements are displayed in Fig. 3.

In Fig. 3, node 50 is connected to the ground and fixed in all degrees of freedom. This node is connected to node 3, which is restricted to free rotation along the local y axis only. Between nodes 50 and 3, a spring can be connected. As an alternative to a spring, a more complicated dynamic system can be connected (e.g., an actuator) that can contain nonlinearities (i.e., free play). The remaining structure is assumed to behave linearly.

Subsequent analysis was performed in the reduced modal domain of the structure, making modal analysis tractable. The unforced natural frequencies and mode shapes were determined, assuming the

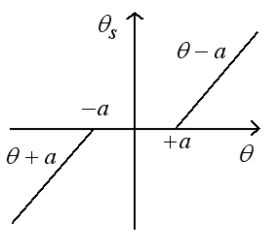

a) The free-play function

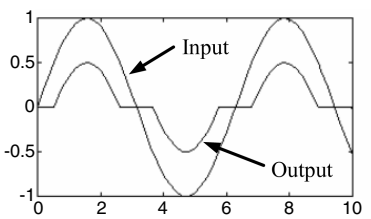

b) Output due to sinusoidal input

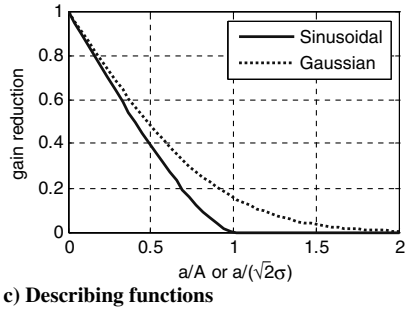

c) Describing functions

Fig. 2 The free-play nonlinearity.

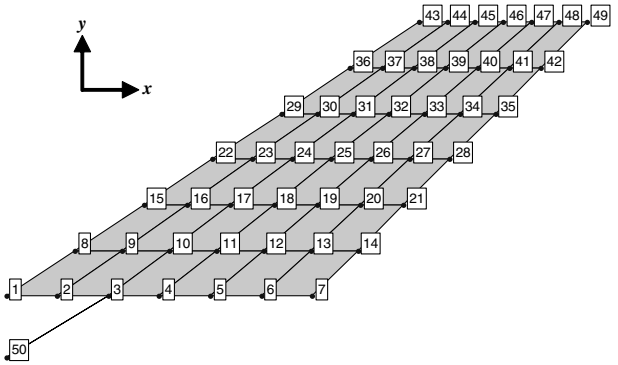

Fig. 3 Stabilator structural model: node locations and plate elements.

quadrilateral plates have identical stiffness and material density properties (although they differ geometrically). The first four mode shapes are displayed in Fig. 4.

B. Unsteady Aerodynamic Model

The forced structural equation of motion for the stabilator model is described by Eq. (1), in which the vector u contains the structural degrees of freedom, M is the structural mass matrix, and K is the structural stiffness matrix:

$$M\ddot{u} + Ku = F \tag{1}$$

In Eq. (1), the force vector F contains the forces and moments that act on the structure at all node points, according to the organization of the global structural degree of freedom vector u. Forces important to the present work are aerodynamic forces, which are generally described by Eq. (2):

$$F = q_\infty Q(\text{Mach}, t, u, \dot{u}, \ddot{u}) \tag{2}$$

In the preceding equation, dynamic pressure is represented by q_∞. Nondimensional forces are assumed unsteady functions of time, as well as functions of shape of the structure and its derivatives. The stabilator is assumed to be undergoing oscillatory motion. This allows use of the unsteady doublet-lattice method [8,9] for calculation of frequency-dependent aerodynamic forces. Implementing the doublet-lattice method, aerodynamic forces are described as

$$Q(\text{Mach}, t, u, \dot{u}, \ddot{u}) = Q(\text{Mach}, \omega, V_\infty, \bar{c})u = Q(\text{Mach}, k)u \tag{3}$$

A further generalization of Eq. (3) allows nondimensionalization by reduced frequency:

$$k = \frac{\omega \bar{c}}{V_\infty} \tag{4}$$

The unsteady doublet-lattice method is used to produce a complex-valued aerodynamic influence coefficient (AIC) matrix, which is a function of reduced frequency k and Mach number. This matrix (denoted AIC) is a function of geometry in the aerodynamic domain and produces a matrix that maps nondimensional aerodynamic downwash velocities to nondimensional forces in the aerodynamic domain:

$$c_p = [\text{AIC}(\text{Mach}, k)]\bar{w} \tag{5}$$

The resultant vector c_p contains local pressure coefficients, and $\bar{w}$ are local nondimensional aerodynamic downwash velocities at control points on respective aerodynamic panels.

Assuming the vertical aerodynamic control point displacements are described by f, the local dimensional downwash vector w_{aero} is described by the following equation:

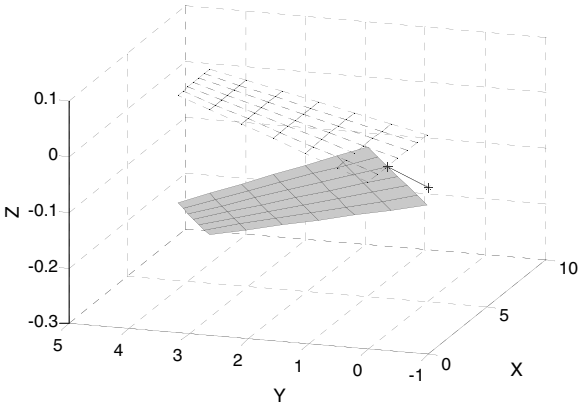

a) Mode 1: frequency of 0 Hz

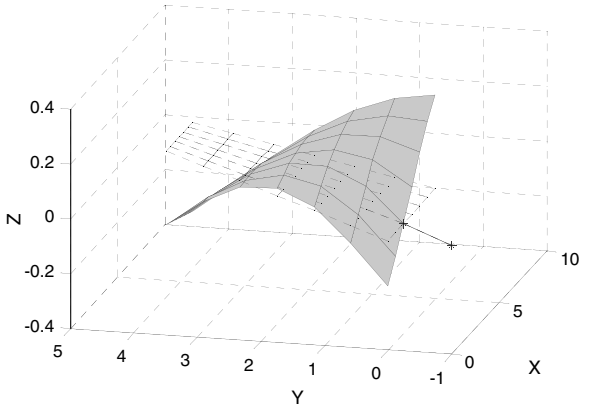

b) Mode 2: frequency of 0.95 Hz

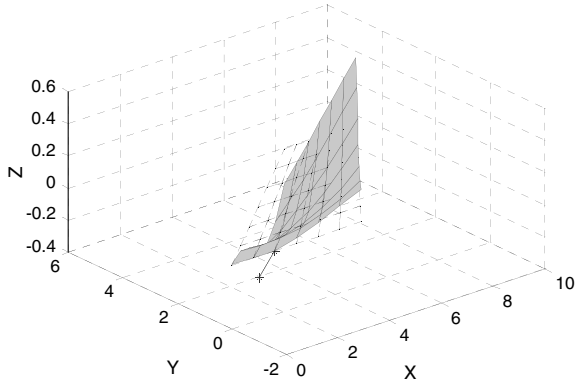

c) Mode 3: frequency of 1.7 Hz

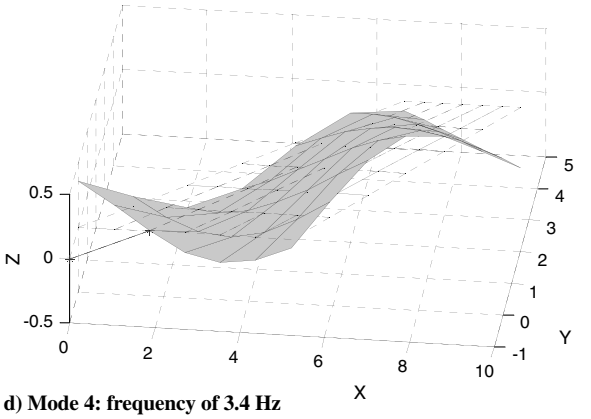

d) Mode 4: frequency of 3.4 Hz

Fig. 4 First four unforced natural mode shapes of the generic stabilator model.

$$w_{\text{aero}} = V_\infty \frac{\partial f}{\partial x} + j\omega f \tag{6}$$

Nondimensionalizing by a characteristic length (mean chord $\bar{c}$), the downwash is described by

$$\bar{w} = \frac{\partial \bar{f}}{\partial \bar{x}} + j\frac{\omega \bar{c}}{V_\infty}\bar{f} = \frac{\partial \bar{f}}{\partial \bar{x}} + jk\bar{f} \tag{7}$$

where $\bar{f} = f/\bar{c}$ and $\bar{x} = x/\bar{c}$.

The aerodynamics are not calculated in the same coordinate system as the structural model because they each require different degrees of accuracy. A transformation between coordinate systems must be defined to allow the structural model to be updated with aerodynamic forces. Translation from aerodynamic coordinates f to structural coordinates u and its inverse is defined in general by the following transformation matrices:

$$f = T_{as}u \qquad u = T_{sa}f \qquad \frac{\partial f}{\partial x} = T_{xas}u \tag{8}$$

These linear transformations (T_{as}, T_{sa}, and T_{xas}) are approximate and are derived and described using equivalent energy methods (refer to [7] for details). Using Eqs. (7) and (8), pressure coefficients in Eq. (5) are rewritten with respect to the structural domain in Eq. (9):

$$\begin{aligned} c_p &= [\text{AIC}(\text{Mach}, k)]\left(\frac{\partial \bar{f}}{\partial \bar{x}} + jk\bar{f}\right) \\ &= [\text{AIC}(\text{Mach}, k)]\left(T_{xas} + \frac{jk}{\bar{c}}T_{as}\right)u \end{aligned} \tag{9}$$

The aerodynamic force on each aerodynamic panel is described as a function of the pressure coefficient, as shown in Eq. (10):

$$F_{\text{aero}} = q_\infty S_{\text{diag}} c_p \tag{10}$$

S_{diag} is a diagonal matrix of aerodynamic panel characteristic areas. The forces in the structural domain are defined by the following:

$$F = T_{sa}F_{\text{aero}} \tag{11}$$

Therefore, the total forces due to aerodynamics, in the structural domain, are defined as

$$\begin{aligned} F &= q_\infty T_{sa} S_{\text{diag}}[\text{AIC}(\text{Mach}, k)]\left(T_{xas} + \frac{jk}{\bar{c}}T_{as}\right)u \\ &= q_\infty Q(\text{Mach}, k)u \end{aligned} \tag{12}$$

The resulting $Q(\text{Mach}, k)$ matrix is similar to a matrix of stability derivatives in which the number of degrees of freedom is significantly larger than states in a traditional rigid-body formulation. The matrix also contains dynamic unsteady information, such as aerodynamic phase lags. The matrix is complex valued and, as a result, the output force can be out of phase with the input deflection reflecting unsteady aerodynamic circulation buildup. For a range of reduced frequency values at a fixed Mach number, a frequency response can be produced. This frequency response is not representative of a linear system but can be approximated as such with high accuracy, depending on prediction methods used. This prediction technique will be described later in this development.

C. Complete Aeroelastic Model

The complete stabilator system is described by Eq. (13):

$$\begin{aligned} M\ddot{u} + Ku &= q_\infty T_{sa} S_{\text{diag}}[\text{AIC}(\text{Mach}, k)]\left(T_{xas} + \frac{jk}{\bar{c}}T_{as}\right)u \\ &= q_\infty Q(\text{Mach}, k)u \end{aligned} \tag{13}$$

Solving the generalized eigenvalue problem, the unforced structural mode shapes are collected into a matrix X. With generalized eigenvectors, the complete equation of motion is cast into modal coordinates:

$$\ddot{u}_m + \Omega_0^2 u_m = q_\infty X^T Q(\text{Mach}, k) X u_m \tag{14}$$

where $u = Xu_m$. This structure has many degrees of freedom. As such, approximating the system with a fixed number of modes is desirable to reduce the system degrees of freedom without a significant loss of accuracy. Implementing this approach, the matrix X is approximated with the first n columns, where n is the number of retained modes for analysis.

1. *Stability Determination: Flutter Points*

The points of instability of the aeroelastic system, which are the flutter points, are computed using Eq. (13). The process is iterative because the aerodynamic forces are calculated in a different domain, with the reduced frequency as an input. Two nominal flutter points were determined for the generic stabilator, representing a case with and without a torsional spring at the hinge (Table 1).

2. *Linear Approximation to the Aerodynamics*

The aerodynamic influence data Q is not in a real rational linear form with respect to the reduced frequency k. It is necessary to construct a complete linear form of the aeroelastic stabilator system without the free-play component(s). To obtain a complete linear form, a real rational approximation of the aerodynamics must be constructed. There are many methods available in the literature [10]. These techniques are primarily based on Roger's method [11]. This method describes the fitting of the AIC data to a multiple-input multiple-output (MIMO) transfer function where the numerator order is higher than the denominator by two. Also, it is assumed that the denominator contains only real-valued stable poles. Because this technique mandates that the denominator poles be real and stable, it makes data fitting challenging because the poles must be estimated a priori. Methods can be conducted where the poles are chosen via nonlinear optimization, which provides good prediction of data. However, this technique is cumbersome and does not guarantee a global minimum. Relaxing the requirement for real-valued poles simplifies the problem substantially.

In this work, a different approach is taken that fits frequency response data to a MIMO transfer function using linear least squares, guaranteeing a global minimum if the requirement for stability is relaxed. The estimated coefficients are those of the transfer function numerator and denominator. Because stability is a strict requirement, a modified technique is applied. This method computes a least-squares solution to estimate the system poles and flips the real part of unstable poles, then a least-squares problem is solved to estimate the zeros, while the poles are fixed to be those found in the previous step. In addition, equality constraints are applied to ensure the frequency response matches exactly at predefined points (e.g., zero frequency to match steady state and at flutter frequencies).

This problem is one of fitting aerodynamic influence [Q in Eq. (13)] to a linear transfer function. Assuming common input dynamics, it is more efficient to fit the rows or columns of Q to multiple-input single-output or single-input multiple-output transfer functions, each with an a priori determined system order. Because this problem is solved in a reduced modal domain, the Q matrix is

Table 1 Nominal flutter points for stabilator with and without a torsional spring at the hinge

Stabilator at Mach 0.3	Flutter point with free hinge	Flutter point with torsional spring at hinge
Altitude	37,570 ft	17,270 ft
Velocity	290 ft/s	314 ft/s
Dynamic pressure	27.8 lb/ft^2	68.65 lb/ft^2
Reduced frequency	0.4515	0.3271
Actual frequency	5.38 Hz	4.22 Hz

reduced, making the problem tractable. The modal matrix $\bar{Q}$ is shown in the equation of motion in Eq. (15):

$$\ddot{u}_m + \Omega_0^2 u_m = q_\infty X^T Q(\text{Mach}, k) X u_m = q_\infty \bar{Q}(\text{Mach}, k) u_m \quad (15)$$

It is noted that the modal matrix $\bar{Q}(k)$ is dependent on Mach number, requiring multiple fits to be performed for varying Mach number. For the work here, the Mach number was assumed constant.

For analysis, five modes were retained, yielding a complex-valued aerodynamic influence coefficient matrix that is 5×5. A fit was performed with these data for a range of reduced frequencies ($0.16 \le k \le 0.90$). The fit was constrained to be exact at a reduced frequency of zero (steady state) and at the reduced frequencies of the two flutter points shown in Table 1. These equality constraints provide for a better fit in the neighborhood of the instability points, which are of primary concern in this development.

3. Complete Linear Representation of the Aeroelastic Stabilator

With a linear representation of the aerodynamic influence coefficient Q, a complete linear system was constructed that describes the motion of the stabilator. The unsteady aerodynamic forces were approximated linearly (as described above) and are represented in state-space form:

$$\bar{Q}(k): \begin{cases} (\bar{c}/V_\infty) E \dot{x} = Ax + Bu_m \\ y = Cx + Du_m \end{cases} \quad (16)$$

The linear representation was with respect to the reduced frequency k and improper transfer functions were allowed in the general formulation. This allowed the descriptor state-space form to be used and dimensionalized by the mean chord and the velocity. The output of the aerodynamic system y is the input to the structural system:

$$\ddot{u}_m + \Omega_0^2 u_m = q_\infty y = q_\infty Cx + q_\infty D u_m \quad (17)$$

The complete system is represented as a first-order state equation:

$$\begin{bmatrix} (\bar{c}/V_\infty)E & 0 & 0 \\ 0 & I & 0 \\ 0 & 0 & I \end{bmatrix} \begin{bmatrix} \dot{x} \\ \ddot{u}_m \\ \dot{u}_m \end{bmatrix} = \begin{bmatrix} A & 0 & B \\ q_\infty C & 0 & q_\infty D - \Omega_0^2 \\ 0 & I & 0 \end{bmatrix} \begin{bmatrix} x \\ \dot{u}_m \\ u_m \end{bmatrix}$$
$$\hat{E}\,\dot{q} = Nq \quad (18)$$

where: $q = [\,x \quad \dot{u}_m \quad u_m\,]^T$. Using this representation, the stability can be determined from the eigenvalues, and simulations can be carried out assuming initial conditions for u_m.

This formulation was used for the stabilator with free rotation at the hinge. Inclusion of the spring is relatively simple. In the structural model, the addition of the spring only affects the stiffness matrix. The global stiffness matrix is written as a sum of nominal stiffness matrix without the spring, plus a stiffness matrix component that contains the spring:

$$K = K_0 + K_{\text{spr}} \quad (19)$$

Projecting onto the same modal basis, this becomes

$$X^T K X = X^T K_0 X + X^T K_{\text{spr}} X \quad \bar{K} = \Omega_0^2 + X^T K_{\text{spr}} X \quad (20)$$

The global spring stiffness matrix K_{spr} is a linear function of a sole parameter, the spring constant k_y. Equation (20) is rewritten with this parameter factored out as

$$\bar{K} = \Omega_0^2 + k_y \bar{K}_{\text{spr}} \quad (21)$$

where:

$$\bar{K}_{\text{spr}} = X^T \hat{K}_{\text{spr}} X \quad \text{and} \quad K_{\text{spr}} = k_y \hat{K}_{\text{spr}}$$

With a new modal stiffness matrix, Eq. (18) becomes a function of the spring constant only, shown as follows:

$$\begin{bmatrix} (\bar{c}/V_\infty)E & & \\ & I & \\ & & I \end{bmatrix} \begin{bmatrix} \dot{x} \\ \ddot{u}_m \\ \dot{u}_m \end{bmatrix} = \begin{bmatrix} A & 0 & B \\ q_\infty C & 0 & q_\infty D - \Omega_0^2 - k_y \bar{K}_{\text{spr}} \\ 0 & I & 0 \end{bmatrix} \begin{bmatrix} x \\ \dot{u}_m \\ u_m \end{bmatrix}$$
$$\hat{E}\,\dot{q} = N(k_y) q \quad (22)$$

Eigenvalues of this matrix define the stability at a given altitude. Assume k_y is a multiplier of the nominal spring constant. The multiplier k_y that drives the system unstable is the reduction (or amplification) in the spring constant that drives the system unstable. For altitudes between the flutter altitude of the free stabilator and the stabilator with a nominal spring attached at the hinge (see Table 1), the system is conditionally stable with respect to the spring. Between the two flutter altitudes, a reduction in the spring constant to a value between zero and one will drive the system unstable.

IV. Aeroelastic Stabilator-Spring System Represented as a Linear Fractional Transformation

The free-play nonlinearity is analyzed via describing function analysis [6]. Because this nonlinearity is simple (i.e., static and frequency independent), it can be approximated as a gain reduction. The free play is placed in series with a spring at the actuator hinge and is approximated as a reduction in the spring constant k_y. An LFT can be used as a standard formulation to separate the spring (or springs) that are in series with free play in feedback. This approach is an excellent means to analyze this problem because it separates the linear components completely from the nonlinear components. Further analysis and simulation with the true nonlinear components can be easily implemented if the system is cast into an LFT. The LFT formulation allows the addition of a more complicated system (i.e., an actuator) with relative simplicity. In addition, it is straightforward to add more complex nonlinearities, such as rate limits or saturations.

The equation of motion for the aeroelastic system including the spring is represented as follows:

$$\ddot{u}_m + \bar{K} u_m = q_\infty Cx + q_\infty D u_m$$
$$\ddot{u}_m + \Omega_0^2 u_m + k_y \bar{K}_{\text{spr}} u_m = q_\infty Cx + q_\infty D u_m \quad (23)$$

Define new signals y_{sp} and w_{sp}:

$$y_{\text{sp}} = \bar{K}_{\text{spr}} u_m \qquad w_{\text{sp}} = k_y y_{\text{sp}} \quad (24)$$

The equation of motion then becomes

$$\ddot{u}_m + \Omega_0^2 u_m + I w_{\text{sp}} = q_\infty Cx + q_\infty D u_m \quad (25)$$

The LFT system, which has $\dot{q}$ and y_{sp} as outputs and q and w_{sp} as inputs, is defined as

$$\begin{bmatrix} (\bar{c}/V_\infty)E & & & \\ & I & & \\ & & I & \\ & & & I \end{bmatrix} \begin{bmatrix} \dot{x} \\ \ddot{u}_m \\ \dot{u}_m \\ y_{\text{sp}} \end{bmatrix} = \begin{bmatrix} A & 0 & B & 0 \\ q_\infty C & 0 & q_\infty D - \Omega_0^2 & -I \\ 0 & I & 0 & 0 \\ 0 & 0 & \bar{K}_{\text{spr}} & 0 \end{bmatrix} \begin{bmatrix} x \\ \dot{u}_m \\ u_m \\ w_{\text{sp}} \end{bmatrix}$$

$$\bar{E} \begin{bmatrix} \dot{q} \\ y_{\text{sp}} \end{bmatrix} = \begin{bmatrix} M_{q'q} & M_{q'w} \\ M_{yq} & M_{yw} \end{bmatrix} \begin{bmatrix} q \\ w_{\text{sp}} \end{bmatrix} \tag{26}$$

The LFT is constructed as illustrated in Fig. 5.

The lower block with Ik_y in feedback is defined as follows:

$$\begin{aligned} \hat{E}\,\dot{q} &= (M_{q'q} + k_y M_{q'w}[I - k_y M_{yw}]^{-1} M_{yq})q \\ &= (M_{q'q} + k_y M_{q'w} M_{yq})q \end{aligned} \tag{27}$$

Notice that, for this system, M_{yw} is zero allowing Eq. (27) to be simplified as shown. The lower LFT is equivalent to $N(k_y)$ in Eq. (22).

V. Estimation of Limit-Cycle Behavior Using Describing Functions

As stated previously, the LFT formulation is used to conveniently separate the nonlinear system components from the linear components. This permits classical describing function analysis to be applied to this general formulation to predict limit-cycle occurrence and amplitude based on nonlinearity size and type.

A. Limit-Cycle Amplitude Prediction

For the following analysis, the altitude chosen was 25,000 ft at a Mach number of 0.3. At this altitude, the system is conditionally stable because it lies between flutter altitudes for no free-play and unlimited free-play cases. At this altitude, the system LFT was driven unstable when the spring was ∼44% of its original value of 1E5 lbs/rad. Based on the sinusoidal describing function, an LCO was predicted with an amplitude of ∼2.2 times the free-play size (Fig. 6). The system response was periodic and, as such, the sinusoidal describing function was used. Other describing functions, which are based on expected input types (i.e., stochastic) may be used in other circumstances deemed appropriate by the expected response and signal type being used as input to the nonlinearity in question.

The destabilizing spring constant multiplier k_y was found using Eq. (27). One of the eigenvalues of the closed-loop system described by this equation crossed into the right half-plane when the spring constant was driven below the critical value. LCO amplitude was predicted according to the describing function shown in Eq. (28) and graphically in Fig. 6 [6]:

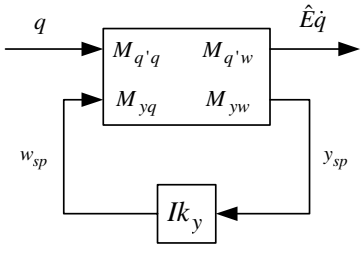

Fig. 5 Aeroelastic stabilator-spring LFT feedback system.

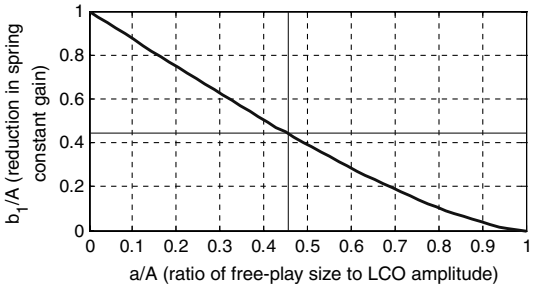

Fig. 6 Free-play sinusoidal describing function solution and prediction of LCO amplitude.

$$\begin{aligned} b_1/A = {} & \frac{1}{\pi}[\pi - 2\sin^{-1}(a/A) + \sin(2\sin^{-1}(a/A))] \\ & - \frac{4}{\pi}(a/A)\cos(\sin^{-1}(a/A)) \end{aligned} \tag{28}$$

B. Validation with Nonlinear Simulation

A simulation was performed with the LFT system replacing the lower block gain (Ik_y in Fig. 5) with a true free play. Simulink™ was used to set up the LFT system and accurately apply the free-play nonlinearity.

For the following example, the simulation was initialized with the stabilator deflected about the hinge with a positive angle of attack of 1 deg. The model had free play at the hinge with a magnitude of ±0.5 deg. The simulation was run for 1500 s. The time series data for the stabilator deflection angle at the hinge is displayed in Figs. 7–11.

These figures show overall time series data followed by detail of regions focused at key points, including transition to limit cycle, limit-cycle transition region, and final limit-cycle region. The nonlinear simulation confirms that a limit cycle is evident. Using describing functions, the estimated LCO amplitude was 2.2 times the size of the free play, which is 1.1 deg. The final limit cycle shows excellent agreement with this prediction (Fig. 11). The amplitude is very close to what was predicted, which confirms the soundness of the prediction using sinusoidal describing functions.

The nonlinear simulation shows two frequencies in the limit cycle and transition region (∼1.4 and ∼16 Hz). A qualitative description of this behavior is provided. The system is unstable inside the free-play bounds. The magnitude of the unstable eigenvalue matches the low

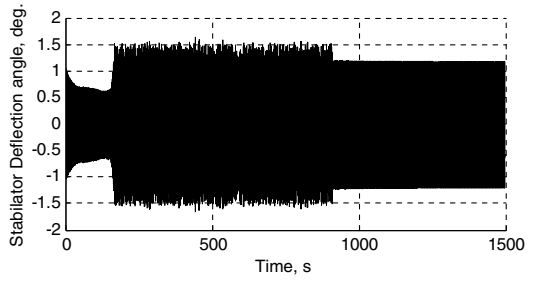

Fig. 7 Stabilator deflection angle at hinge time history: nonlinear simulation.

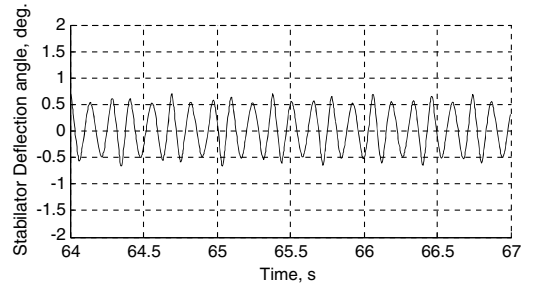

Fig. 8 Stabilator deflection angle at hinge time history: nonlinear simulation (detail before limit-cycle transition).

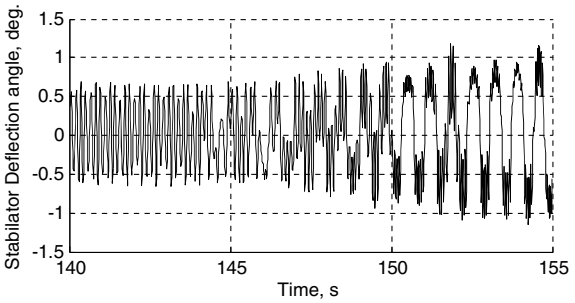

Fig. 9 Stabilator deflection angle at hinge time history: nonlinear simulation (detail of transition to limit cycle).

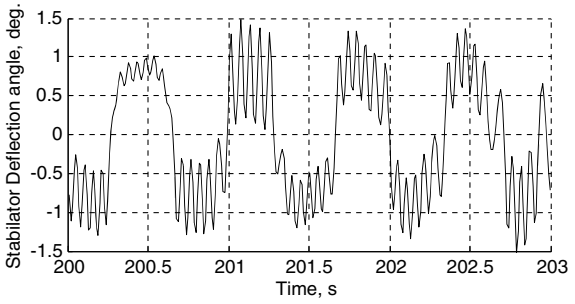

Fig. 10 Stabilator deflection angle at hinge time history: nonlinear simulation (detail of limit-cycle transition region).

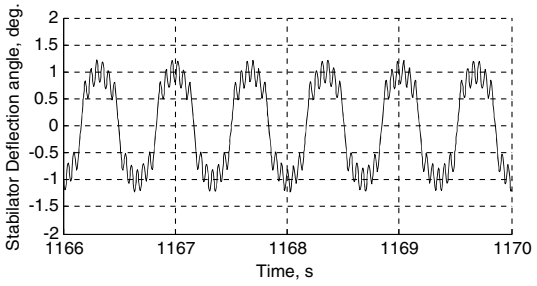

Fig. 11 Stabilator deflection angle at hinge time history: nonlinear simulation (detail of final limit-cycle region).

frequency present (∼1.4 Hz). The high frequency present in the limit cycle is due to the spring at the hinge. When the system encounters the free-play boundary of ±0.5 deg, the dynamics abruptly change and a high-frequency, lightly damped pole appears. This frequency is excited by an impulsive step change when the system encounters this boundary. The systems differ slightly in the low-frequency range. A significantly higher frequency pole appears outside the free-play threshold. This frequency is ∼19 Hz, which is very close to the ∼16 Hz oscillation observed in the nonlinear simulation.

C. Analysis of Frequency Content in Time Series Data

In addition to describing function analysis, time series data from the nonlinear simulation (Fig. 7) were used to determine frequency content. Wavelets are used with the time series data to estimate a time-varying power spectral density (PSD), showing dominant frequencies present in the response [12]. A scalogram plot was used to visualize these data (Fig. 12).

Figure 12 depicts a mesh of the power spectral density as a function of time. For ∼100 s, a single dominant frequency of ∼7 Hz is present. At ∼150 s simulation time, the PSD transitions to a dominant frequency of ∼1.4 Hz with a higher less-dominant frequency of ∼16 Hz.

This time series data and subsequent frequency content analysis successfully display the presence of a nonlinearity. For a linear time-invariant system, the scalogram would show no change in dominant

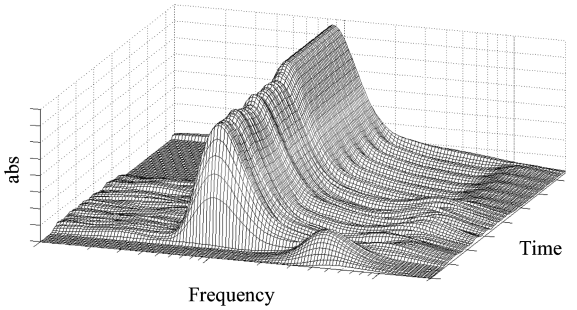

Fig. 12 Scalogram showing frequency power as a function of time: mesh representation.

frequencies. The PSD magnitude may change, but the location of the magnitude with respect to frequency would remain constant. The presence of a nonlinearity is characteristic of frequency shifts or new frequencies introduced as a function of time. In addition to nonlinearity presence, an LCO can be qualitatively determined from a scalogram as well. A limit cycle is characterized by a constant magnitude PSD as a function of time. This frequency shift and constant magnitude PSD behavior is clearly evident in the scalogram in Fig. 12.

VI. Relevance to Models of Increasing Complexity

The stabilator model used in this study is of medium complexity. It is more complex than a simple two-dimensional pitch–plunge model, but is less complex than a high-fidelity model represented with a large number of finite elements and complex Euler- or Navier–Stokes-based computational fluid dynamics (CFD). The analysis described here is general and can be applied to problems with much more complexity. For instance, the equations of motion [Eq. (1)] is representative of a general aeroelastic system in which the structure can be represented by a larger FE model and aerodynamic forces can be determined from a more complex CFD formulation. The significant characteristic of the methods presented here is that the aerodynamic forces must be described or approximated linearly. The method to obtain a linear aerodynamic approximation used in this work was done by fitting the AIC forces to a linear transfer function. There are several alternative methods to this approach in which the accuracy is dependent on the technique used to characterize the aerodynamic forces. For higher-order complex CFD models, examples of linear reduced-order modeling (ROM) include proper orthogonal decomposition [13–16], Volterra [17–20], and system identification methods [11,21–23]. Raveh has authored a comprehensive summary of these methods [24]. These model reduction and simplification methods have been shown to produce accurate linear ROMs even in highly complex fluid regimes (including the troublesome transonic regime). Once a ROM is determined, the computational burden for analysis is significantly reduced and the resulting linear model can be used conveniently for further analysis and stability determination, including application to the aeroservoelastic model presented in this work.

A significant aspect to this formulation is the LFT. Traditionally used as a tool to aid uncertainty analysis in feedback systems [25], the LFT has seen increasing exposure applied to nonlinear system analysis and nonlinear system identification [26]. The advantage of the LFT as applied to this formulation is the construction of a form that is of significant generality, in which the nonlinear elements in question (i.e., the free play) are separated from the linear elements. Analysis assuming this general formulation is performed independent of inner complexities of the model. Classical describing function analysis is applied efficiently and accurately to determine important characteristics, such as limit-cycle occurrence and behavior. Moreover, nonlinear simulations are applied with ease using the LFT formulation. It is expected that this LFT formulation will see increased use in further analysis of complex nonlinear aero(servo) elastic systems, including the inverse problem, in which the free-play nonlinearity can be estimated from time series data.

VII. Conclusions

Excessive free play in aeroservoelastic systems cause limit-cycle oscillations, which may be detrimental to handling qualities, ride qualities, and aircraft structural life. Because of these consequences, military specifications for free-play size are stringent unless it can be shown through extensive analysis and testing that the requirements can be relaxed. Methods using describing functions and linear fractional transformations have been presented as analysis tools that are computationally efficient and provide necessary accuracy to alleviate or justify these requirements. These analysis techniques have been demonstrated with the use of a finite element and unsteady aerodynamic model of an aeroelastic stabilator control surface with free play at the actuator hinge.

The techniques presented in this paper accurately and efficiently analyze and characterize free play in aeroelastic systems. These tools can be used to obtain a better understanding of free-play effects and provide accurate predictions of limit-cycle oscillation behavior. As such, these analysis methods can be used to alleviate or enforce restrictive requirements set forth for the purposes of flight performance and flight safety.

Acknowledgments

The work described herein was conducted as part of a Phase I Small Business Innovation Research program sponsored by the NASA Langley Research Center in conjunction with the NASA Dryden Flight Research Center. The authors acknowledge NASA for valuable resources and funding to make this project possible.

References

[1] Hoffman, N. R., and Spielberg, I. N., "Subsonic Flutter Tests of an Unswept All-Moveable Tail," Wright Air Development Center WADC-TR-54-53, Wright-Patterson AFB, Dayton, OH, 1954.

[2] Cooley, D. E., "Subsonic Flutter Model Tests of a Low Aspect Ratio Unswept All-Moveable Tail," Wright Air Development Center WADC-TR-58-31, Wright-Patterson AFB, Dayton, OH, 1958.

[3] "Department of Defense Joint Service Specification Guide—Aircraft Structures," JSSG-2006, 30 Oct. 1998.

[4] Roskam, J., *Airplane Design Part IV: Layout Design of Landing Gear and Systems*, Roskam Aviation and Engineering Copdrp., Ottawa, KS, 1989, pp. 236–237.

[5] Kiiskila, J. C., Duncan, M. R., and Pitt, D. M., "Investigation of the Dynamic Characterization of Aircraft Control Surface Free Play," *Proceedings of the 24th International Modal Analysis Conference*, St. Louis, MO, 30 Jan. 2006–2 Feb. 2006.

[6] Graham, D., and McRuer, D. T., *Analysis of Nonlinear Control Systems*, Wiley, New York, 1961, pp. 77–143.

[7] Przemieniecki, J. S., *Theory of Matrix Structural Analysis*, Dover, New York, 1985, pp. 115–122, 305–309.

[8] Albano, E., and Rodden, W. P., "A Doublet-Lattice Method for Calculating Lift Distributions on Oscillating Surfaces in Subsonic Flows," *AIAA Journal*, Vol. 7, No. 2, Feb. 1969, pp. 279–285. doi:10.2514/3.5086

[9] Rodden, W. P., Taylor, P. F., and Mcintosh, S. C., "Further Refinement of the Subsonic Doublet-Lattice Method," *Journal of Aircraft*, Vol. 35, No. 5, 1998, pp. 720–727. doi:10.2514/2.2382

[10] Tiffany, S. H., and Karpel, M., "Aeroservoelastic Modeling and Applications Using Minimum-State Approximations of the Unsteady Aerodynamics," NASA TM-101574, April 1989.

[11] Roger, K. L., "Airplane Math Modeling Methods for Active Control Design," *Structural Aspects of Active Controls*, AGARD CP-228, Aug. 1977, pp. 4.1–4.11.

[12] Mitchell, D. G., and Klyde, D. H., "Identifying a Pilot-Induced Oscillation Signature: New Techniques Applied to Old Problems," *Journal of Guidance, Control, and Dynamics*, Vol. 31, No. 1, 2008, pp. 215–224. doi:10.2514/1.31470

[13] Dowell, E. H., "Eigen-Mode Analysis in Unsteady Aerodynamics: Reduced-Order Models," *Proceedings of the AIAA 36th Structures, Structural Dynamics, and Materials Conference*, AIAA, Washington, DC, 1995, pp. 2545–2557.

[14] Silva, W., Beran, P., Cesnik, C., Guendel, R., Kurdila, A., Prazenica, R., Librescu, L., Marzocca, P., and Raveh, D., "Reduced-Order Modeling: Cooperative Research and Development at the NASA Langley Research Center," *Proceedings of the CEAS International Forum on Aeroelasticity and Structural Dynamics*, Vol. 2, Madrid, Spain, June 2001, pp. 159–174.

[15] Beran, P., and Silva, W. A., "Reduced-Order Modeling—New Approaches for Computational Physics," *39th AIAA, Aerospace Sciences Meeting and Exhibit*, AIAA Paper 2001-0853, Reno, NV, Jan. 2001.

[16] Lieu, T., Farhat, C., and Lesoinne, M., "Modeling of a Complete Aircraft Configuration," *Computer Methods in Applied Mechanics and Engineering*, Vol. 195, Nos. 41–43, 2006, pp. 5730–5742. doi:10.1016/j.cma.2005.08.026

[17] Silva, W. A., "Reduced-Order Models Based on Linear and Nonlinear Aerodynamic Impulse Responses," *AIAA 40th Structures, Structural Dynamics, and Materials Conference*, AIAA Paper 99-1262, St. Louis, MO, April 2002.

[18] Raveh, D. E., "Reduced-Order Models for Nonlinear Unsteady Aerodynamics," *AIAA Journal*, Vol. 39, No. 8, 2001, pp. 1417–1429. doi:10.2514/2.1473

[19] Reisenthel, T. J., "Prediction of Unsteady Aerodynamic Forces via Nonlinear Kernel Identification," *CEAS/AIAA/ICASE/NASA Langley International Forum on Aeroelasticity and Structural Dynamics*, NASA Langley Research Center, Williamsburg, VA, 22–25 June 1999.

[20] Prazenica, R., Kurdila, A., and Silva, W.A., "Multiresolution Methods for Representation of Volterra Series and Dynamical Systems," *41st AIAA/ASME/ASCE/AHS/ASC Structures, Structural Dynamics, and Materials Conference*, AIAA Paper 2000-1754, Atlanta, April 2000.

[21] Ballhaus, W. F., and Goorjian, P. M., "Computation of Unsteady Transonic Flows by Indicial Methods," *AIAA Journal*, Vol. 16, No. 2, 1978, pp. 117–124. doi:10.2514/3.60868

[22] Cowan, T. J., Arena, A. S. Jr., and Gupta, K. K., "Accelerating Computational Fluid Dynamics Based Aeroelastic Predictions Using System Identification," *Journal of Aircraft*, Vol. 38, No. 1, 2001, pp. 81–87. doi:10.2514/2.2737

[23] Silva, W., and Bartels, R., "Development of Reduced-Order Models for Aeroelastic Analysis and Flutter Prediction Using the CFL3Dv6.0 Code," *AIAA 43rd Structures, Structural Dynamics, and Materials Conference*, AIAA Paper 2002-1596, Denver, CO, April 2002.

[24] Raveh, D. E., "Computational-Fluid-Dynamics-Based Aeroelastic Analysis and Structural Design Optimization—A Researcher's Perspective," *Computer Methods in Applied Mechanics and Engineering*, Vol. 194, Nos. 30–33, 2005, pp. 3453–3471. doi:10.1016/j.cma.2004.12.027

[25] Zhou, K., Doyle, J. C., and Glover, K., *Robust and Optimal Control*, Prentice–Hall, Upper Saddle River, NJ, 1996, pp. 213–300.

[26] Hsu, K., Poolla, K., and Vincent, T. L., "Identification of Structured Nonlinear Systems," *IEEE Transactions on Automatic Control*, Vol. 53, No. 11, 2008, pp. 2497–2513. doi:10.1109/TAC.2008.2006928